

Scalar field confinement as a model for accreting systems

M. Megevand¹, I. Olabarrieta^{1,2}, L. Lehner¹

¹ Department of Physics and Astronomy, Louisiana State University,
202 Nicholson Hall, Baton Rouge, Louisiana 70803-4001, USA

² TELECOM Unit, ROBOTIKER-Tecnalia, Ed. 202 Parque Tecnológico Zamudio E-48170, Bizkaia, SPAIN

(Dated: October 27, 2018)

We investigate the possibility to localize scalar field configurations as a model for black hole accretion. We analyze and resolve difficulties encountered when localizing scalar fields in General Relativity. We illustrate this ability with a simple spherically symmetric model which can be used to study features of accreting shells around a black hole. This is accomplished by prescribing a scalar field with a coordinate dependent potential. Numerical solutions to the Einstein-Klein-Gordon equations are shown, where a scalar field is indeed confined within a region surrounding a black hole. The resulting spacetime can be described in terms of simple harmonic time dependence.

I. INTRODUCTION

Self-gravitating scalar field configurations have been very useful in many aspects of gravitational theory. Their role as describing matter models (eg.[1, 2, 3, 4, 5]); as governing mechanisms to model inflationary scenarios (eg. [6, 7]); as probes of strong curvature regions (eg.[8, 9]), etc. has made them an ideal tool in a number of fronts. In this work we examine exploiting scalar fields to mimic some salient properties of accreting black hole systems. To this end, it is desirable to explore a configuration where the scalar field simulates an accretion disk surrounding a black hole. For this purpose, one should be able to confine the scalar field within some compact region surrounding the black hole. Since massless scalar fields radiate away to infinity, the model sought after should include a mechanism that will prevent this from happening, at least to some non-trivial extent. (The existence of bound states for particular cases in spherical symmetry are studied in [10, 11]).

One way to confine the scalar field would be by employing a potential well which would introduce some sort of barrier and thus allow for confinement. The use of carefully chosen potentials is common practice with scalar fields, and are usually functions of the field itself. Examples of this kind of potential are the quadratic ($V(\phi) \propto \phi^2$) –that introduces a mass term–; and the quartic ($V(\phi) \propto \phi^4$). However, that kind of potential does not allow for confining the scalar field within a specific region of space, that one can specify *a priori*.

What we are looking for is a potential that somehow depends on the coordinates and in particular can be chosen to describe a potential well within a region. However, this proposition seems *a priori* at odds with maintaining covariance. The difficulty one encounters with a coordinate-dependent potential, is that the corresponding stress-energy tensor is in general inconsistent, in the sense that its divergence will not be zero for a non-trivial scalar field. This fact, together with the Einstein equations, would imply that the Bianchi identities are not satisfied.

Faced with this situation a possible way of confining the scalar field would be to introduce a background with

respect to which coordinates could be defined. This approach would be in line with bi-metric theories of gravity (eg.[12]). Another approach would be to fix a suitable coordinates already at the level of the action as is done in [13] through some suitably introduced Lagrange multipliers. This procedure then provides a way to covariantly adopt coordinates which could, in principle, be used in the potential. However, this method would strongly link the adopted gauge with the type of potential introduced and it is not yet clear whether it can be made of practical use. An alternative way, which is the one we pursue here, is to exploit symmetry considerations without resorting to introducing any other feature in the problem. The existence of the symmetry provides a simple way to consistently introduce a coordinate-dependent potential in the problem. Certainly, while more restricted than other possible viable options, this approach is the more direct one. A particular case of a coordinate dependent potential has already been implemented in [14, 15] to effectively simulate angular momentum in spherical or axial symmetry.

In this work we concentrate mainly on the case of spherical symmetry, but give prescriptions for the implementation of potentials in both spherical and axial symmetry. We will see that, if the space is spherically symmetric, we can implement a potential that depends on the areal radius. In the same way, for an axially symmetric spacetime, the potential can depend on the length of the closed integral curves defined by the associated killing vector. Even though one will not be able to specify the potential as an arbitrary function of any coordinate, one may still be able to confine a scalar field to some region, as is it shown in this work for the case of spherical symmetry. This fact will become apparent in section II A and in its applications in the rest of this work.

This paper is organized as follows. In section II, we study the specification of a stress-energy tensor for a scalar field with a coordinate dependent potential. Showing that such implementation is possible when the spacetime possesses a symmetry. In particular, the case of spherical symmetry is studied in depth (we also consider an axi-symmetric case in an appendix). In section III we

describe the formulation used, and the resulting equations. In section IV we discuss how the equations are solved numerically, after obtaining initial data by two different methods. In section V we show and analyze the numerical solutions obtained, finding that, after some transient behavior, the scalar field reaches a state described by a simple harmonic time dependence and remains confined to a region surrounding the black hole. We have confirmed these for initial masses of the scalar field up to 50% of that of the black hole. Finally, we make some final remarks in section VI. In all this work we use Einstein's index notation and geometrized units.

II. SCALAR FIELD ON A COORDINATE-DEPENDENT POTENTIAL

In this section we study the specification of a stress-energy tensor for a scalar field with a coordinate dependent potential. Our motivation is to somehow confine a scalar field within a region around a black hole. The resulting system would share features of a black hole interacting with an accretion disk. We will see that this can be done when the space-time possesses a symmetry. However, the specification of such potential is not completely arbitrary since it must depend on the coordinates only through some particular function. Knowing the approximate dependence of that function on the coordinates, one can then construct a potential that confines the scalar field.

Before presenting our approach, we include an overview of how the equations of motion are obtained from a stress-energy tensor in the case of a coordinate-independent potential. Then, based on that procedure, we will study the generalization to the case of a coordinate-dependent potential.

The equations of motion for a real scalar field ϕ on a coordinate-independent potential can be derived from the stress-energy tensor

$$T_{ab} = T^{(k)}_{ab} + T^{(p)}_{ab}, \quad (1)$$

where, for later convenience, we have split this tensor into what we call the “kinetic” and “potential” terms:

$$T^{(k)}_{ab} \equiv (\nabla_a \phi)(\nabla_b \phi) - \frac{1}{2} g_{ab} (\nabla_c \phi)(\nabla^c \phi), \quad (2)$$

$$T^{(p)}_{ab} \equiv -\frac{1}{2} g_{ab} V(\phi). \quad (3)$$

The kinetic part, $T^{(k)}_{ab}$, corresponds to a massless scalar field without a potential.

The equations of motion can be obtained [1, 16] through the condition

$$\nabla_a T^a_b = 0, \quad (4)$$

which must be satisfied to be consistent with a covariant theory. Equation (4) can be re-expressed with $\nabla_b \phi$ as a

common factor,

$$0 = \nabla_a T^a_b = (\nabla_b \phi) \mathcal{L}(\phi), \quad (5)$$

where $\mathcal{L}(\phi)$ contains second order derivatives of ϕ . The equations of motion for a non-trivial scalar field is then

$$\mathcal{L}(\phi) = 0. \quad (6)$$

For example, for $V(\phi) = m^2 \phi^2$ we obtain the Klein-Gordon equation,

$$\mathcal{L}(\phi) \equiv (\nabla_a \nabla^a - m^2) \phi = 0. \quad (7)$$

This is analogous to the Lagrangian approach, where the variation of the action is set to zero, and, after integrating by parts, the integrand becomes $\delta\phi\mathcal{L}(\phi)$.

After this detour, we now turn our attention back to the case of interest, the implementation of a coordinate-dependent potential. Our discussion is based on the precedent one though now generalizing it to the case of a coordinate-dependent potential $V(x^c, \phi)$.

A naive first approach would be to replace occurrences of $V(\phi)$ in (3) by $V(x^c, \phi)$. However, this will bring an unfortunate consequence, namely that one can now no longer express the divergence of T^a_b in the form given by eqn (5), where $\nabla_b \phi$ appears as a common factor. Instead one has

$$0 = \nabla_a T^a_b = (\nabla_b \phi) \left(\nabla_a \nabla^a \phi - \frac{1}{2} \frac{\partial}{\partial \phi} V(x^c, \phi) \right) - \frac{1}{2} \frac{\partial}{\partial x^b} V(x^c, \phi). \quad (8)$$

The crucial difference with eqn. (5) is that several (independent) equations must be satisfied by the real scalar field ϕ . As a result, the system of equations will be generically inconsistent.

To resolve this problem we start by: (i) adopting a different ansatz for $T^{(p)}_{ab}$ (equation (9) below), and (ii) imposing symmetry conditions on the scalar field.

First, consider setting $T^{(p)}_{ab}$, instead of being given by equation (3), to be the product of a function of ϕ and a coordinate dependent tensor,

$$T^{(p)}_{ab} \equiv H_{ab}(x^c) f(\phi), \quad (9)$$

where the function f is independent of x^c and the tensor H_{ab} is independent of ϕ . Now, find a suitable H_{ab} such that $\nabla_a T^a_b$ takes the form of equation (5), this will induce conditions on H_{ab} . Under this choice the divergence of the stress-energy tensor results

$$\nabla_a T^a_b = (\nabla_b \phi) \nabla_a \nabla^a \phi + \frac{\partial f}{\partial \phi} (\nabla_a \phi) H^a_b + f(\phi) \nabla_a H^a_b. \quad (10)$$

Now, we look for conditions that would allow us to express the *r.h.s.* of equation (10) in such a way that $\nabla_b \phi$ appears as a common factor. Since H^a_b is independent

of ϕ , $\nabla_b\phi$ cannot appear in the last term of (10); Then, that term must be zero, resulting in the first condition on H^a_b ,

$$\nabla_a H^a_b = 0. \quad (11)$$

We now consider the second term in the *r.h.s.*; the condition

$$(\nabla_a\phi) H^a_b = (\nabla_b\phi) h(x^c), \quad (12)$$

for some scalar $h(x^c)$, ensures that that term has $\nabla_b\phi$ as a common factor. Equation (12) is satisfied for any scalar field ϕ if

$$H^a_b = h(x^c)\delta^a_b. \quad (13)$$

However, this condition, together with equation (11), implies that $h(x^c)$ is a constant. This means that $T^{(p)}_{ab}$ is of the form (3) (with V independent of x^c). Thus, for an arbitrary scalar field, and without any further structure in the spacetime, space-dependent potentials can not be considered. However, by imposing further conditions on the scalar field ϕ , H^a_b can indeed be chosen with further structure than that of equation (13) while still satisfying equation (12). To this end, we consider[34] the tensor H^a_b of the form

$$H^a_b = h(x)\delta^a_b + A^a_b. \quad (14)$$

Replacing (14) into (12) we find

$$(\nabla_a\phi)A^a_b = 0. \quad (15)$$

The simplest case is the one with $A^a_b = 0$ for which H^a_b is given by (13). More general cases arise when ϕ is independent on one of the coordinates, lets say $\partial_{x^3}\phi \equiv \nabla_3\phi = 0$. Here one can adopt A^3_3 arbitrarily and set all other components to zero, thus satisfying equation (15).

In this particular case, H^a_b takes the form

$$H^a_b = \begin{bmatrix} h & 0 & 0 & 0 \\ 0 & h & 0 & 0 \\ 0 & 0 & h & 0 \\ 0 & 0 & 0 & b \end{bmatrix} \quad (16)$$

for some functions $h(x^c)$ and $b(x^c)$.

Similarly, when ϕ does not depend on two of the coordinates, lets say $\partial_{x^2}\phi = 0$, $\partial_{x^3}\phi = 0$, one can choose

$$H^a_b = \begin{bmatrix} h & 0 & 0 & 0 \\ 0 & h & 0 & 0 \\ 0 & 0 & b & 0 \\ 0 & 0 & 0 & c \end{bmatrix}. \quad (17)$$

Analogous results are obtained when some of its derivatives are linearly related. For example, if $\partial_{x^3}\phi = c\partial_{x^2}\phi$, one can adopt A^3_3 arbitrarily and set $A^2_3 = -cA^3_3$ keeping all other components zero. With this choice, equation (15) will be satisfied and H^a_b will then be given in terms of two functions $h(x^c)$ and $b(x^c)$ in a slightly

different way as is (16).

Summarizing, we have seen that a coordinate dependent potential can be implemented if the following conditions are satisfied: (i) its derivatives are linearly dependent (this includes the possibility of one or more of them being zero). (ii) The ‘‘potential’’ part of the stress-energy tensor is given by (9), with H^a_b satisfying $\nabla_a H^a_b = 0$ and being expressible in the form (16), (17), or similar expressions depending on how condition (i) is fulfilled.

In the next section we will consider in detail the case of spherical symmetry.

A. Spherical Symmetry

We will now concentrate on the case of spherical symmetry. The line element can be written in the form

$$ds^2 = -N^2 dt^2 + g_{rr}(dr + \beta dt)^2 + g_\Omega d\Omega^2, \quad (18)$$

where N , g_{rr} , β , and g_Ω are functions of t and r . We assume that we can adopt coordinates so that $\partial_\theta\phi = \partial_\varphi\phi = 0$. Then, H^a_b is given by (17), with the additional condition that $b = c$ due to the spherical symmetry. H^a_b is then

$$H^a_b = \begin{bmatrix} h & 0 & 0 & 0 \\ 0 & h & 0 & 0 \\ 0 & 0 & b & 0 \\ 0 & 0 & 0 & b \end{bmatrix}, \quad (19)$$

with h and b functions of t and r .

The evaluation of $\nabla_a H^a_b$ gives rise to non-trivial equations only on the t and r components,

$$\frac{dg_\Omega}{dt}(h-b) + 2g_\Omega \frac{dh}{dt} = 0, \quad (20)$$

$$\frac{dg_\Omega}{dr}(h-b) + 2g_\Omega \frac{dh}{dr} = 0. \quad (21)$$

In order to obtain a family of solutions to these equations we will demand that h depends on the coordinates only through g_Ω : $h(t, r) = h(g_\Omega(t, r))$. With this condition, we have that

$$\frac{dh}{dx^i} = \frac{\partial h}{\partial g_\Omega} \frac{dg_\Omega}{dx^i} \quad (22)$$

for $x^i = (t, r)$. Substituting this into either equation (20) or (21), we obtain an expression for b in terms of h ,

$$b = h + g_\Omega \frac{\partial h}{\partial g_\Omega}. \quad (23)$$

We have just seen that, if h depends on the coordinates only through g_Ω , and b is given in terms of h by (23), the prescription (19) for the tensor H^a_b allows us to express $\nabla_a T^a_b$ with $\nabla_b\phi$ as a common factor. More explicitly:

$$\nabla_a T^a_b = (\nabla_b\phi) \left(\nabla_a \nabla^a \phi + \frac{\partial f}{\partial \phi} h(g_\Omega) \right). \quad (24)$$

Notice that, if one wanted to calculate $\nabla_a T^a_b$ without setting $\partial_\theta \phi = \partial_\varphi \phi = 0$ at the onset, one would obtain (24), but with $h(g_\Omega)$ replaced by $b(g_\Omega)$ for the angular components $\nabla_a T^a_\theta$ and $\nabla_a T^a_\varphi$. However, because those terms are actually multiplied by zero, equation (24) is true for all four components.

Setting the *r.h.s* of (24) to zero we obtain the equation of motion for ϕ ,

$$\nabla_a \nabla^a \phi + \frac{\partial f}{\partial \phi} h(g_\Omega) = 0, \quad (25)$$

where we remind the reader that f is an arbitrary function of ϕ , and h is an arbitrary function of g_Ω .

Throughout the rest of this work we will choose these functions as

$$f(\phi) = -\frac{1}{2}\phi^2, \quad (26)$$

$$h(g_\Omega) = m^2 + V(g_\Omega). \quad (27)$$

We do that, so that the equation of motion for the scalar field becomes

$$(\nabla_a \nabla^a - m^2 - V(g_\Omega)) \phi = 0, \quad (28)$$

where we interpret the function $V(g_\Omega(t, r))$ as a (coordinate-dependent) potential. The parameter m is set to zero in our simulations. The function $g_\Omega(t, r)$ is just the square of the areal radius, $R(t, r)$. Then, we can write (28) in the form

$$(\nabla_a \nabla^a - m^2 - \tilde{V}(R)) \phi = 0, \quad (29)$$

where \tilde{V} is an arbitrary function of the areal radius.

In appendix A we summarize the results obtained in the case of axial symmetry.

III. THE EQUATIONS

In this work we solve the non-vacuum Einstein equations for a dynamic spherically symmetric space time, coupled to a real scalar field. The scalar field satisfies a Klein-Gordon-like equation with the addition of a potential, as explained in section II A.

The equations are decomposed using a Cauchy formulation, in which the space-time is foliated by space-like surfaces. The particular formulation used is the Einstein-Christoffel hyperbolic formulation [17], where the equations are decomposed into a system of first order hyperbolic “evolution equations,” plus a system of (first order) “constraint equations.” These equations can be solved by giving initial data that satisfy the constraint equations on a given surface of the foliation, and then integrating the evolution equations in time. The constraint equations at later times are then automatically satisfied [16] in the domain of dependence of that surface.

The equations solved are the Einstein-Klein-Gordon equations, with the addition of a potential,

$$G_{ab} = 8\pi T_{ab} \quad , \quad (30)$$

$$(\nabla_a \nabla^a - V) \phi = 0 \quad , \quad (31)$$

where the stress-energy tensor, T_{ab} , and the potential, V , are given according to section II A, as well as the condition that ϕ is independent of (θ, ϕ) . In equation (31) we have set $m = 0$, but this parameter can be incorporated in the definition of V .

We consider the line element and extrinsic curvature of a space time in spherical symmetry in the form

$$ds^2 = -N^2 dt^2 + g_{rr}(dr + \beta dt)^2 + r^2 g_T d\Omega^2 \quad (32)$$

$$K_{ij} dx^i dx^j = K_{rr} dr^2 + r^2 K_T d\Omega^2, \quad (33)$$

where β is the (r component of the) shift vector, and N is the lapse function. In the Einstein-Christoffel formulation, the shift and “densitized lapse” function, $\alpha \equiv N/\sqrt{g}$, are arbitrarily specified and kept fixed during the evolution. We denote by g the determinant of the three-metric.

In spherical symmetry, this system reduces to nine first order evolution equations, and four first order constraint equations, the later containing only spatial derivatives.

The variables evolved are: the metric components, g_{rr} and g_T ; the scalar field, ϕ ; and other variables used to convert the equations from second to first order. They are: the extrinsic curvature components, K_{rr} and K_T (defined in eqn.(33)); variables $\{\Psi, \Pi\}$ constructed with first-derivatives of ϕ ,

$$\Psi = \partial_r \phi, \quad (34)$$

$$\Pi = \frac{1}{N} (\beta \partial_r \phi - \partial_t \phi); \quad (35)$$

and the variables $\{f_{rrr}, f_{rT}\}$ containing first spatial derivatives of the metric,

$$f_{rrr} = \frac{\partial_r g_{rr}}{2} + \frac{4g_{rr} f_{rT}}{g_T}, \quad (36)$$

$$f_{rT} = \frac{\partial_r g_T}{2} + \frac{g_T}{r}. \quad (37)$$

The complete expressions of these equations are shown in detail in appendix B. Their derivation, and the notation used, is based on [18] and [19], with the addition of terms containing the potential.

IV. NUMERICAL IMPLEMENTATION

A. Initial Data

Consistent initial data must satisfy equations (B12)-(B16). These equations determine some variables in terms of others judiciously chosen. In this work, we exploit this freedom to describe a black hole centered

at $r = 0$ by specifying $\{V, \phi, g_{rr}, K_{rr}\}$ from the known Schwarzschild solution and solving for g_T and K_T .

Before describing the details of our implementation, we discuss how the potential and scalar field are chosen. We adopt a potential V with two free parameters $\{A, r_0\}$ to regulate the depth and location of the “well” where the scalar field is to be confined (see figure 1). A simple expression for V suffices for this task, and we adopt

$$V(R) = A \left(1 - e^{-(R-r_0)^2}\right), \quad (38)$$

with the areal radius R given by $R = r\sqrt{g_T}$. The parameters in this expression were set to $A = 30/M^2$ and $r_0 = 6M$, where M is the initial mass of the black hole. Notice that during the evolution $R = R(t, r)$, thus, in these coordinates, the shape (and position) of the potential well can change in time. We will return to this point later.

The scalar field ϕ is defined following either one of two different strategies. One is designed to conform to time-harmonic situations in weakly-gravitating cases and the other simply prescribing a sufficiently smooth profile. The latter choice allows us to investigate the space-time’s response to fields not designed to conform to a time-harmonic dependence.

1. Time-harmonic scalar field

To prescribe a scalar field which will give rise to a spacetime with harmonic time-dependence, we begin by considering the limiting case when the scalar field’s amplitude is negligible; there the metric should be described by the Schwarzschild’s solution. Now, considering the scalar field as existing over this fixed background spacetime, a Schrödinger-like eigenvalue equation can be obtained to determine time-harmonic states as discussed below.

The Schwarzschild metric in Eddington-Finkelstein coordinates is:

$$ds^2 = -\left(1 - \frac{2M}{r}\right) dt^2 + \left(1 + \frac{2M}{r}\right) dr^2 + \frac{4M}{r} dt dr + r^2 d\Omega^2. \quad (39)$$

We use this metric to evaluate the equation of motion for ϕ , equation (31). To solve this PDE we use the following ansatz that yields separation of variables[35],

$$\phi(t, r) = u(r) \cos\left(\omega \left[t - 2M \ln\left(\frac{r-2M}{M}\right)\right]\right). \quad (40)$$

The equation for $u(r)$ results

$$\mathcal{L} u(r) = \left[\omega^2 - \left(1 - \frac{2M}{r}\right) V(r)\right] u(r), \quad (41)$$

where the second order operator \mathcal{L} is given by

$$\mathcal{L} = -\left(1 - \frac{2M}{r}\right)^2 \frac{\partial^2}{\partial r^2} - \frac{2}{r} \left(1 - \frac{M}{r}\right) \left(1 - \frac{2M}{r}\right) \frac{\partial}{\partial r} \quad (42)$$

Equation (41) is integrated to obtain $u(r)$. Then, from its definition, equation (40), $\phi(t, r)$ is calculated. Finally, from $\phi(t, r)$ we obtain $\Pi(t, r)$ and $\Phi(t, r)$ evaluating these functions at $t = 0$ and adopting them as initial data.

Equation (41) can be straightforwardly integrated to obtain both the eigenvalue and eigenfunction through a standard shooting algorithm. To this end, we transform the second-order equation to a system of two first order equations for $u(r)$ and $u'(r) \equiv du/dr$ augmented with a third equation $((\omega^2)') = 0$ to simplify the implementation (see [20] for the details).

The system of equations is then integrated outwards from $r_L \equiv 4M$ on one hand, and also inwards from $r_R \equiv 8M$. The obtained solutions are matched at an intermediate point, in our case at r_0 (the center of the potential well), with the conditions that both the solutions and derivatives are continuous. The initial guesses for the boundary conditions are then varied until a satisfactory match is obtained. The code used to implement the shooting algorithm is the one described in [20], except that the ODE integrator is replaced for LSODE (Livermore Solver for ODEs) [21]. The boundary conditions, consistent with the physical scenario in mind are determined as follows.

We have a system of three first order ODEs, thus three boundary conditions need be specified. Natural conditions for our purposes result from requiring the fields fall sufficiently rapid at the boundaries. We thus impose a relationship between u and its derivative at each boundary, of the form $u' = ku$. The coefficient k at each boundary can be found through a WKB-type approach. To do so, we first consider the variable change $u(r) \equiv F(r)\tilde{u}(r)$ and fix $F(r) = [r(r-2M)]^{-\frac{1}{2}}$ so as to remove the first order derivative in equation (41). The resulting equation is

$$-f(r)\tilde{u}''(r) + V_{\text{eff}}(r)\tilde{u}(r) = \omega^2\tilde{u}(r) \quad (43)$$

with $f(r)$ and $V_{\text{eff}}(r)$,

$$f(r) = \left(1 - \frac{2M}{r}\right)^2, \quad (44)$$

$$V_{\text{eff}}(r) = \left(1 - \frac{2M}{r}\right) V(r) - \frac{M^2}{r^4}, \quad (45)$$

and we interpret V_{eff} as an effective potential (which is shown in figure 1). Next, we freeze the coefficients $f(r)$ and V_{eff} on a small neighborhood of each boundary point and consider solutions of the form $\exp(\pm kr)$, with $k^2 = (V_{\text{eff}} - \omega^2)/f$. The following conditions at the boundaries are then determined by

$$\tilde{u}(r) \propto e^{+k_1 r} \quad \text{at } r = r_L, \quad (46)$$

$$\tilde{u}(r) \propto e^{-k_2 r} \quad \text{at } r = r_R, \quad (47)$$

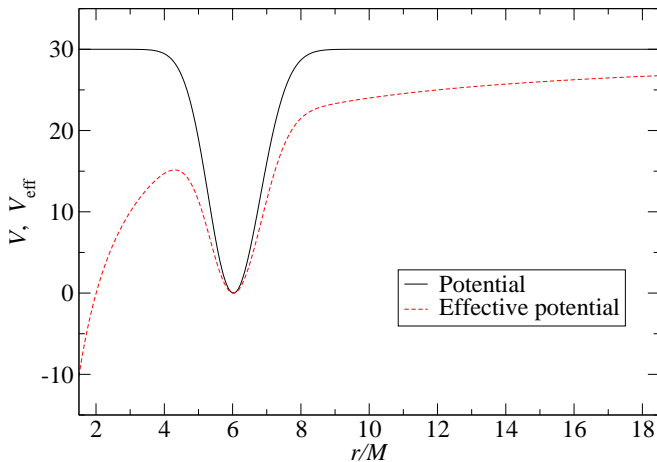


FIG. 1: Potential and effective potential, as defined in (38) and (45), respectively. As mentioned in the text, the potentials are, in general, functions of $R \equiv r\sqrt{g_T}$. The potentials showed in this figure are those used to find the time harmonic states $u(r)$, where the Schwarzschild metric is used, hence $R = r$.

where

$$k_1 = \sqrt{\frac{V_{\text{eff}}(r_L) - \omega^2}{f(r_L)}}, \quad (48)$$

$$k_2 = \sqrt{\frac{V_{\text{eff}}(r_R) - \omega^2}{f(r_R)}}. \quad (49)$$

As illustrated later, these conditions indeed ensure the solutions decay rapidly outside of the potential well (for a bounded range of values of ω^2). Notice that since the equations are homogeneous there remains a freedom on the amplitude of the fields at the boundaries. We fix this freedom by setting $u = 1$ at r_L and adopting as the varying parameter for the shooting method the value of u at r_R .

Once obtained $\phi(r)$ in $[r_L, r_R]$ using equation (40), we set $\phi(r) = 0$ outside this region. For the amplitude of ϕ used in this work in the case of time-harmonic initial data, the values of ϕ and its derivative at r_L and r_R are small enough to ensure that this matching is sufficiently smooth, as is corroborated when evolving these initial data.

2. Smooth profile

The other approach employed in this work is to adopt a simple expression for the scalar field. In particular we adopt a “pulse” of compact support of the form

$$\phi(r) = \begin{cases} c(r - r_1)^4(r - r_2)^4 & r_1 \leq r \leq r_2 \\ 0 & \text{elsewhere} \end{cases}, \quad (50)$$

where the values r_1 and r_2 control the width of the pulse and were chosen so that it is centered with the potential

(at $r = 6M$): $r_1 = 5M$, $r_2 = 7M$. After specifying r_1 and r_2 , the coefficient c is chosen so that the scalar field has a given mass. This initial data is used to compare with the previous approach in regimes where the fixed-background approximation is justified and to study the spacetime’s behavior in non-linear cases.

Remaining data

Having specified both the potential and the scalar field, consistent initial data is determined by integrating the constraint equations in the following manner. First, the functions g_{rr} , K_{rr} , α , and β are set equal to those read-off from the Schwarzschild solution in Eddington-Finkelstein coordinates. Adopting these coordinates gives the freedom to place the inner boundary inside the black hole. We found it convenient to rewrite the constraint equations in the form:

$$\partial_r g_T = d_T, \quad (51)$$

$$\partial_r d_T = f_1(g_T, d_T, K_T; F_i), \quad (52)$$

$$\partial_r K_T = f_2(g_T, d_T, K_T; F_i), \quad (53)$$

where F_i represents all the functions that are specified a priori (including ϕ). These equations are integrated outwards from the inner boundary using the step adaptive integrator LSODE, using as boundary data (g_T , d_T , and K_T at $r = r_{\min}$) the values read-off from the Schwarzschild solution.

B. Evolution

We discretize the equations with a scheme formulated to take advantage of numerical techniques which guarantee stability of generic linear first order hyperbolic systems. In this work we adopt: (i) second order accuracy by implementing second-order derivative operators satisfying summation by parts [22, 23, 24, 25, 26]; (ii) a third-order Runge-Kutta operator for the time integration through the method of lines [27]; (iii) a Kreiss-Oliger [28] style dissipative algorithm to control the high frequency modes of the solution [26, 29, 30] and (iv) maximally dissipative boundary conditions setting all incoming modes to zero [29, 31].

We employ a uniform grid to cover the region $r \in [r_{\min}, r_{\max}]$ with N equi-spaced points. The grid-spacing between points is $\Delta r = (r_{\max} - r_{\min})/(N - 1)$. The time step Δt is defined in terms of Δr as $\Delta t = cfl \Delta r$ and $cfl = 0.25$ is chosen so that the CFL condition [32] is satisfied. In what follows, sub-indices denote particular points of a slice, and super-indices distinguish each slice.

The inner boundary, $r = r_{\min}$, is set inside the black hole initially, and monitored during the evolution to ensure that it remains inside and constitutes an outflow boundary of the computational domain. Then, there is no need to prescribe boundary conditions there. At the

outer boundary, $r = r_{\max}$ maximally dissipative boundary conditions are adopted. In our present case we take the simplest form of these conditions and set the incoming modes to zero. The characteristic structure for the system of equations is detailed in appendix C.

The code have been tested to ensure that the numerical solutions obtained converge to the corresponding solutions of the Einstein equations. In appendix D we show the convergence test for the Hamiltonian constraint.

V. ANALYSIS AND RESULTS

In the simulations performed in this work we set the initial mass of the black hole to $M = 1$ (in geometrized units). The domain of integration was chosen so that the region of interest is unaffected by the conditions adopted at the right boundary. This corresponds to $r_{\min} = 1M$ and $r_{\max} = 221M$. The maximum resolution used was $\Delta r = 0.01M$ (22000 grid points).

In the two approaches we use to obtain initial data, we have the freedom of adjusting the amplitude of the scalar field, which in turn determines its mass. We set initial data where the mass of the scalar field is $m_{\text{sf}} = 0.01M$ in the time-harmonic case, while for the non-time-harmonic cases we set m_{sf} equal to $0.01M$, $\kappa 0.1M$, (M being the initial mass of the black hole and $\kappa = 1\dots 5$). To calculate the mass we use the Misner-Sharp formula [1],

$$M_{\text{MS}}(r) = \frac{r\sqrt{g_T}}{2} \left[1 + \frac{r^2}{g_T} \left(K_T^2 - \frac{f_{rT}^2}{g_{rr}} \right) \right], \quad (54)$$

which measures the total mass inside a spherical surface labeled by coordinate r . In our initial data the mass of the black hole, M , is preset, so we can calculate m_{sf} by subtracting M from the total mass of the space-time,

$$m_{\text{sf}} = M_{\text{MS}}(R) - M, \quad (55)$$

where R labels a sphere containing the scalar field, which is localized initially. (See figure 8).

During the evolution we employ this formula, replacing M for M_{MS} at the horizon[36].

In our analysis we also evaluate the Kretschmann invariant $I \equiv R_{abcd}R^{abcd}$, where R_{abcd} is the Riemann tensor. This quantity provides a gauge-invariant answer that can be compared with its value in known spacetimes. For a Schwarzschild space-time, I is given by

$$I_{\text{Sch}} = \frac{48(M_{\text{MS}})^2}{R^6}, \quad (56)$$

where, in Schwarzschild coordinates, $M_{\text{MS}} = M$ and $R = r$. We evaluate the quotient I/I_{Sch} using (56) with $R = r\sqrt{g_T}$ and M_{MS} defined in (54).

A. Initial Data

As explained in section IV A 1, we first find time-harmonic states for the scalar field on a Schwarzschild

space-time. By varying the initial guess for the frequency in the shooting integration we obtain different modes. We show the first modes in figures 2 and 3. However, for this work we used only the first mode which will be referred to as “the time-harmonic state”, unless otherwise specified. These modes have been re-scaled so that they can be normalized (in analogy with quantum mechanics) so that $\int r^2 |u(r)|^2 dr = 1$. There is no physical justification for choosing that particular normalization, but it is helpful when comparing different eigenstates, which otherwise would have greatly different amplitudes.

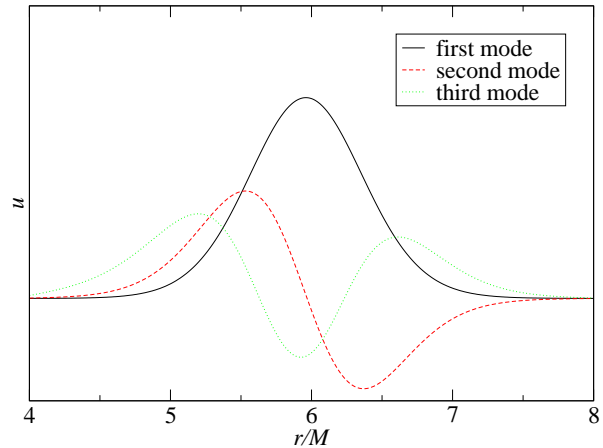


FIG. 2: First time-harmonic states of $u(r)$.

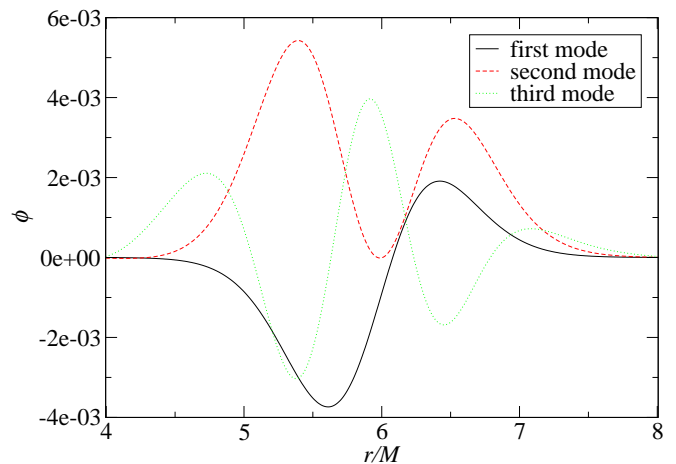


FIG. 3: Scalar field at $t = 0$ obtained from the first time-harmonic states of $u(r)$, using equation (40).

The other approach used to define the initial data corresponds to the “pulse” described in section IV A 2. In the linear regime we employ both types of initial data, with a scalar field’s initial mass $m_{\text{sf}} = 0.01M$. In the non-linear regime we adopt only the non-time-harmonic initial data with masses m_{sf} ranging from $0.1M$ to $0.5M$.

B. Evolution

We study the evolution of the prescribed data. We begin by considering first the linear regime, adopting scalar field configurations with initial mass of 1% of that of the black hole. After confirming that the time-harmonic configuration behaves as expected, we confirm that the “pulse” configuration evolves towards a time-harmonic regime. Then, we study cases in the non-linear regime, with initial scalar field masses ranging from 10% to 50% of that of the black hole. In all cases we evolve until $t = 200M$.

Linear case

The time-harmonic initial data constructed essentially remains unchanged through the evolution while the non-time-harmonic data evolves towards a time-harmonic state. Figures 4 and 5 illustrate $\phi(r)$ at different times for the maximum resolution employed ($\Delta r = M/100$). Figure 4 corresponds to the time-harmonic initial data, and figure 5 to non-time-harmonic initial data. In both cases we sampled along two different periods at $t \approx 80M$; and then at $t \approx 160M$. The corresponding pairs, are then plot together illustrating how after 22 periods apart the solutions are essentially the same. This is further illustrated in figure 6 where we show the difference between each of these pairs for three different resolutions.

Finally, figure 7 displays the absolute value of the Fourier transform in time of $\int \phi dr$, denoted $|F[\phi]|$. The scalar field is first integrated in space, then a discrete Fourier transform in t is calculated, where t ranges from 0 to $200M$ in the case of time-harmonic initial data, and from $t_0 = 60M$ to $200M$ in the non-time-harmonic case. In the plot we also indicate the frequencies ($f_n = \omega_n/2\pi$) obtained from the shooting integration when calculating the time-harmonic states. The time t_0 is chosen after the initial transient behavior, indicated by a time-harmonic behavior observed in ϕ . The initially non-time-harmonic scalar field relaxes to a superposition of the first three time-harmonic modes, the first one being the dominant one. We point out here that for this configuration, the shooting method gives raise to three possible modes. It is thus no surprising that the evolution gives rise to a solution described by these modes. Deeper potentials give rise to more modes.

Figures 8 and 9 show the Misner-Sharp mass function (equation (54)) for both types of initial data. The continuous line shows the initial value (M_{MS} at $t = 0$). The discontinuous lines show M_{MS} at $t = 200M$ for three different resolutions. In both cases the asymptotic value of the mass stays constant, indicating no scalar field energy is radiated away. An inspection of the mass behavior at smaller radii for the solution obtained with time-harmonic initial data reveals that this converges to essentially the initial value, thus a negligible amount of mass falls into the black hole. For the non-time-harmonic case

about 10% of the field’s initial mass falls into the black hole.

The amount of mass that falls into the black hole is calculated by subtracting the Misner-Sharp mass at the horizon, minus the initial mass of the black hole. In the case of time-harmonic initial data this number is $(1 \pm 3) \times 10^{-4}M$, while for that of non-time-harmonic initial data it is $(10 \pm 3) \times 10^{-4}M$ (see table I and figure 14). These values are calculated using the highest resolution ($\Delta r = 1/100M$), and the errors as the difference of these values with those of a lower resolution ($\Delta r = 1/50M$).

Non-linear case

We turn now to the non-linear cases investigated. These correspond to initial mass configurations where the scalar field has a mass of at least 10% of that of the black hole. In this regime we solely adopt the “pulse” prescription defined in equation (50) for the scalar field since the time-harmonic data is obtained under an assumption which is no longer valid.

As we have done for the linear case, we also compare profiles at different times for simulations with higher initial m_{sf} . Figures 10 and 11 correspond to initial masses of the scalar field of $m_{sf} = 0.10M$ and $m_{sf} = 0.50M$, respectively. The time it takes to reach a state described by a harmonic time dependence is longer than in the linear regime, especially for the higher initial $m_{sf} = 0.50M$. For that reason, the first samplings (labeled t_1 in the figures) occur later than in the linear case, and the interval between the profiles compared, $t_2 - t_1$, is ten periods, as opposed to 22 in the linear cases.

The absolute value of the Fourier transform of $\int \phi dr$, $|F[\phi]|$, is shown in figure 12 for the two different initial masses of ϕ . Again, we compute the transformation after the initial transient behavior has passed and the scalar field has already reached a quiescent state. As a useful indicator, we also show the frequencies corresponding to time-harmonic states. Now, while the observed modes do not coincide exactly with those obtained at the linear approximation, they are close to them.

In figure 13 we show the Misner-Sharp mass at $t = 0$; and at $t = 200M$ for three different resolutions. Figures 13(a) and 13(b) correspond to initial masses of the scalar field of $m_{sf} = 0.10M$ and $m_{sf} = 0.50M$, respectively. In all these cases about 10% of the scalar field’s mass falls into the black hole, while nothing escapes outwards. Additionally, for the case with grater mass, the scalar filed spreads slightly outwards before reaching a quiescent state. Although we only show figures corresponding to two different initial values of m_{sf} , we have simulated the system for other values of this parameter $m_{sf} = \kappa 10^{-1}M$ ($\kappa = 1..5$). In all these cases essentially no scalar field energy is radiated away, while a small portion falls into the black hole. The measured values are shown in table I and figure 14.

If, after some transient time, the scalar field is finally

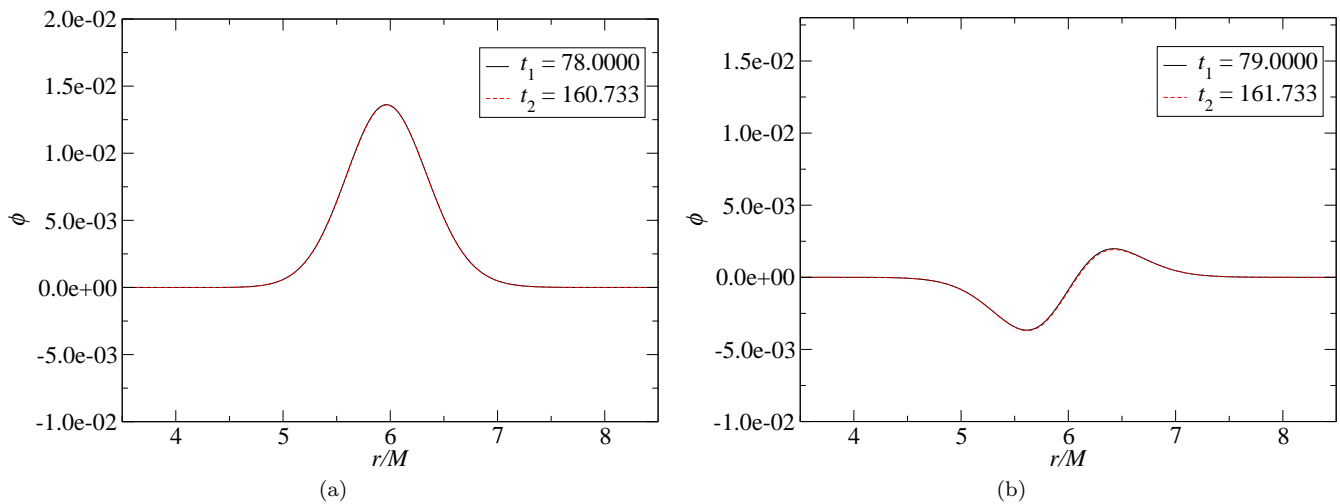


FIG. 4: The scalar field at different times is compared to check if the evolution remains described by a time-harmonic dependence. Case with time-harmonic initial data. Initial mass of the scalar field $m_{\text{sf}} = 0.01M$. Figure 4(a) shows the scalar field when it reaches a maximum, while figure 4(b) shows it at about a quarter of a period later. In both cases, the profile shown in continuous line is separated 22 periods from the one in dashed line.

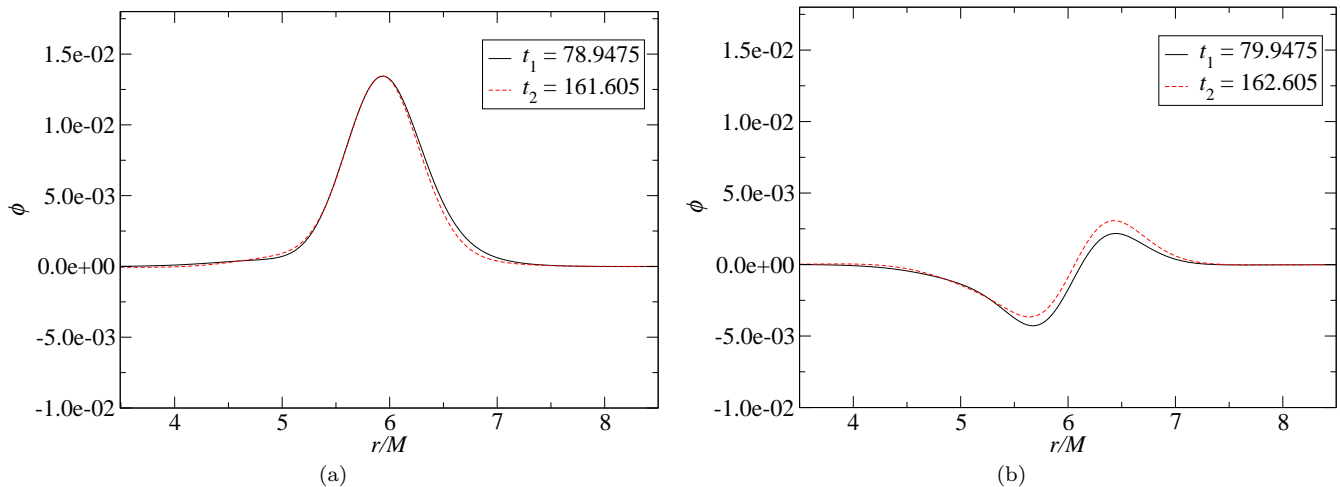


FIG. 5: Here we show the same comparison of profiles as in figure 4, this time for the case with non-time-harmonic initial data. The separation between the profiles compared is also 22 periods. The initial mass of the scalar field is $m_{\text{sf}} = 0.01M$.

TABLE I: Mass that falls into the black hole for different initial masses of the scalar field. Calculated as the Misner-Sharp mass at the horizon at $t = 200$ minus the initial mass of the black hole. See figure 14.

Initial $m_{\text{sf}} [M]$	$(M_{\text{MS}}(r_{\text{h}}) - M) [10^{-2} M]$
0.01	0.10 ± 0.03
0.10	1.0 ± 0.3
0.20	2.9 ± 0.7
0.30	3 ± 1
0.40	5 ± 1
0.50	7 ± 2

confined within a compact region, lets say $[r_a, r_b]$, the space-time should be that of Schwarzschild for $r > r_b$, with a Schwarzschild mass equal to the total mass inside the sphere $r = r_b$. This can be checked by evaluating the Kretschmann invariant. In figure 15 we show the quotient I/I_{Sch} (see the paragraph containing equation (56)) at $t \approx 140M$ for the case with initial $m_{\text{sf}} = 0.5M$. This quotient converges to one for $r > r_b$, and also for $r < r_a$.

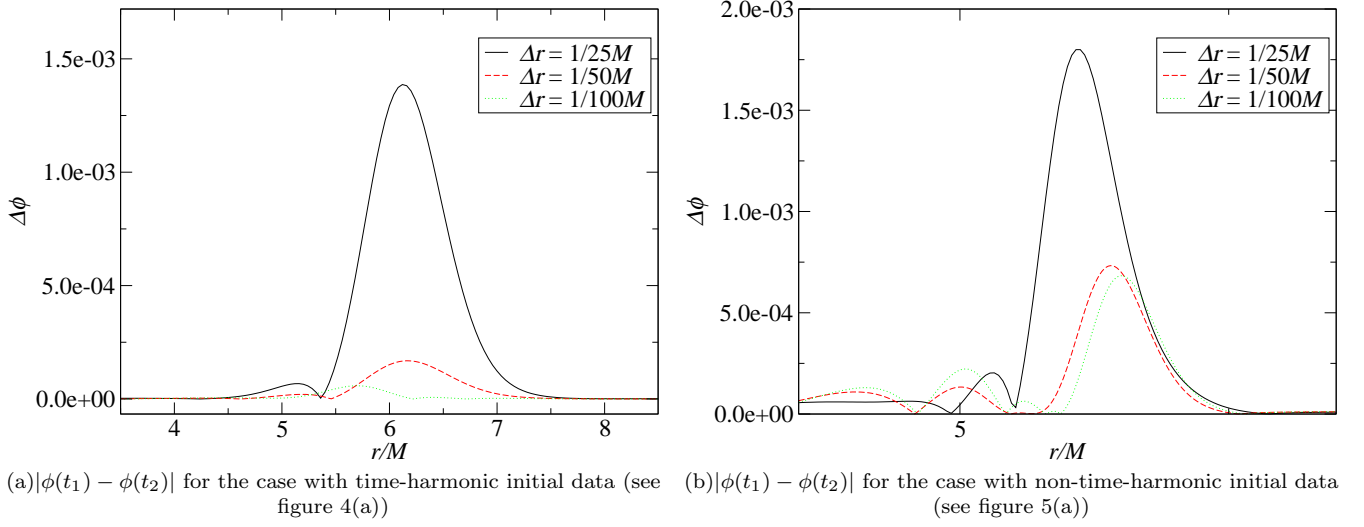


FIG. 6: Absolute value of the difference between the scalar field at different times: $|\phi(t_1) - \phi(t_2)|$, where $t_2 - t_1 = 22$ periods. Figure 6(a) shows the difference between the profiles shown in figure 4(a), while figure 6(b) shows the difference between those in figure 5(a). In each case, we show these differences for three resolutions.

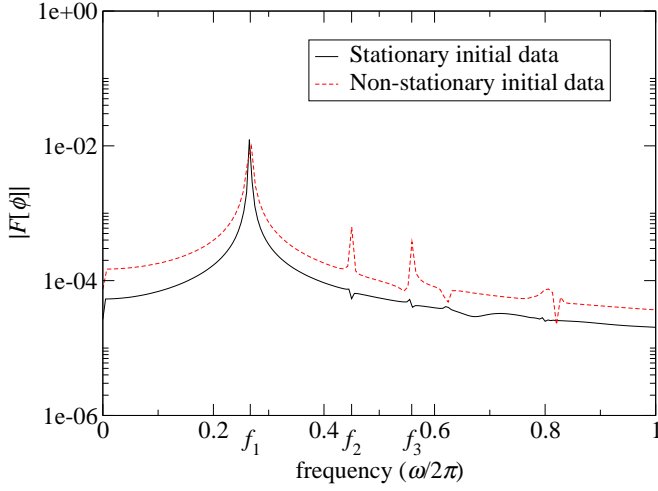


FIG. 7: Absolute value of the discrete Fourier transform in time of $\int \phi dr$. The continuous line corresponds to the time-harmonic initial data, while the dashed line corresponds to the non-time-harmonic initial data. In the later case, the scalar field relaxes to a superposition of the first time-harmonic modes, whose frequencies are shown in the figure (labeled f_n).

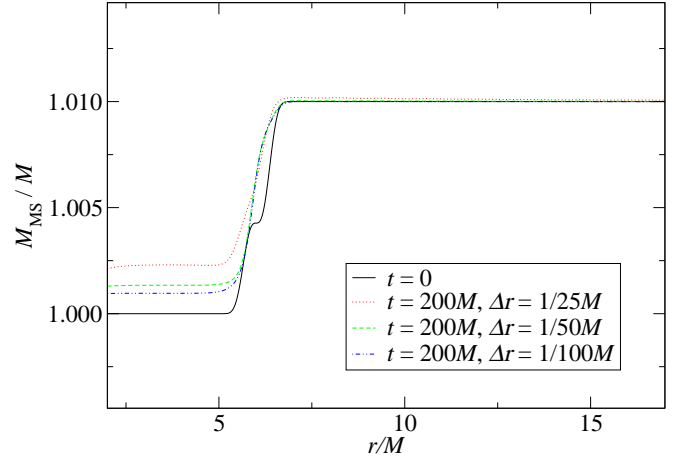


FIG. 9: As in fig. 8, we show the mass function, this time for the non-time-harmonic case. The initial mass of the scalar field is $m_{\text{sf}} = 0.01M$. This time about 10% of it falls into the black hole.

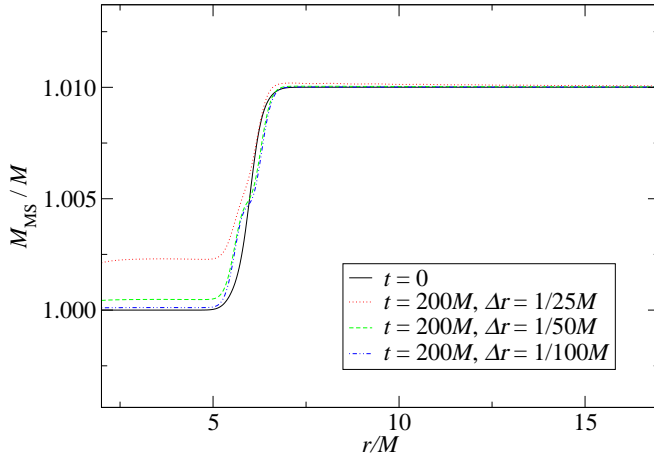


FIG. 8: Mass function at $t = 0$; and at $t = 200M$ for three resolutions. Stationary initial data. Initial $m_{\text{sf}} = 0.01M$. The continuous line shows the mass function at $t = 0$, while the discontinuous lines show, for different resolutions, the mass function at $t = 200M$. In this case the escape of mass into the black hole is negligible ($\Delta m_{\text{sf}} = (1 \pm 3) \times 10^{-4}M$).

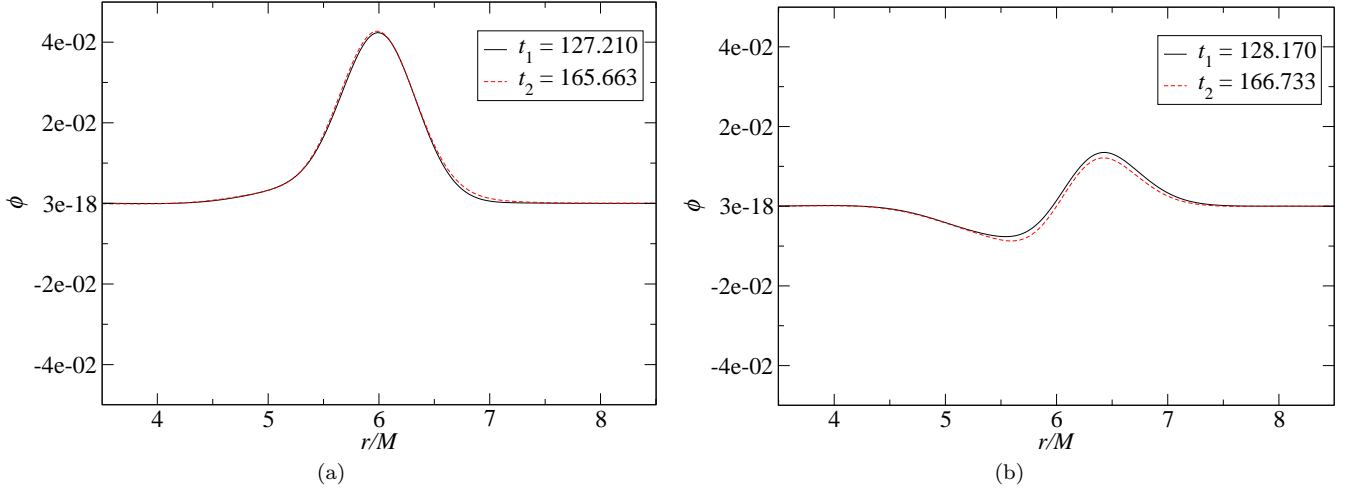


FIG. 10: The scalar field at different times is compared to check if the solution obeys a harmonic time dependence. Case with non-time-harmonic initial data. Initial mass of the scalar field $m_{\text{sf}} = 0.10M$. Figure 10(a) shows the scalar field when it reaches a maximum, while figure 10(b) shows it at about a quarter of a period later. In both cases, the profile shown in continuous line is separated 10 periods from the one in dashed line.

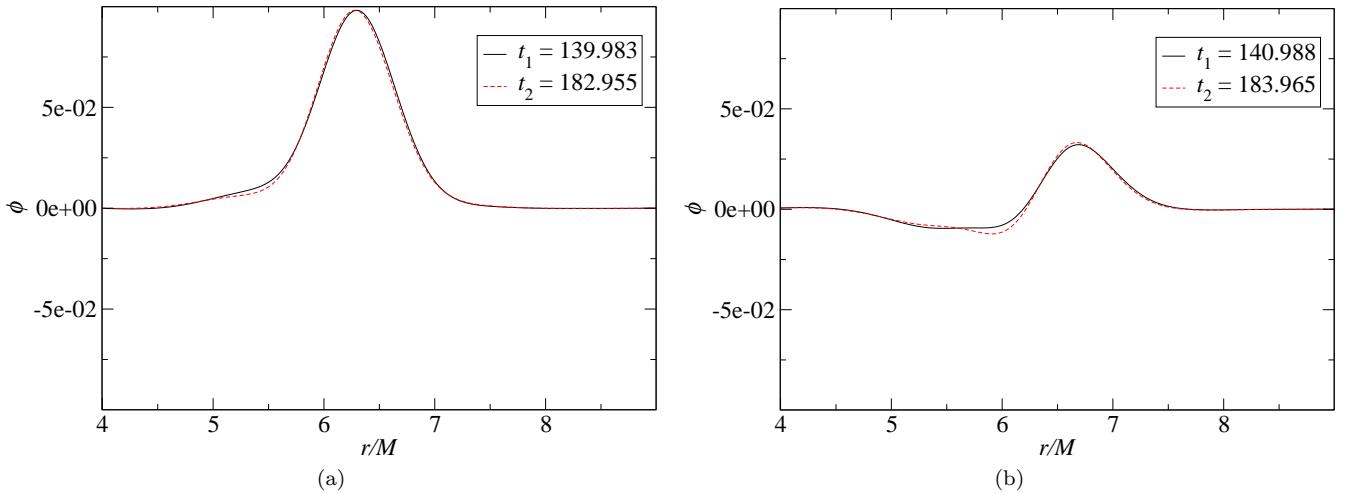


FIG. 11: This figure shows the same comparisons as figure 10, but for an initial mass of the scalar field of $m_{\text{sf}} = 0.50M$. The separation between the profiles compared is also 10 periods.

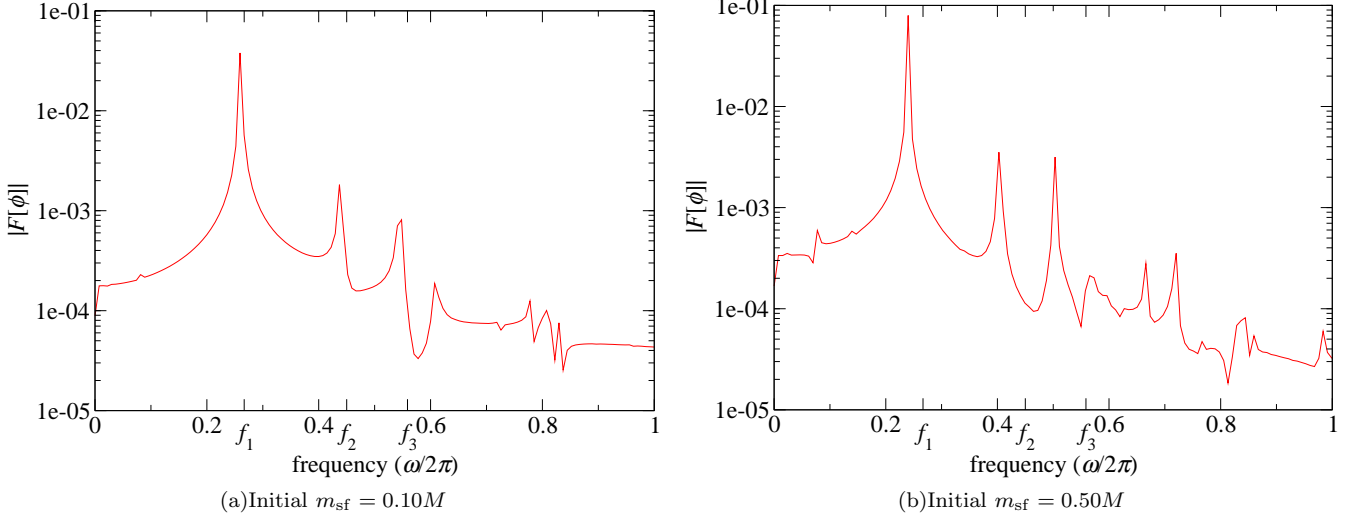


FIG. 12: Absolute value of the discrete Fourier transform in t of the space integral $\int \phi(r, t) dr$. The marks labeled f_n denote the frequencies of the first modes obtained from the shooting. The three peaks, which indicate the dominant frequencies in the solution, lie at slightly lower frequencies than those of the time-harmonic states in the linear case. This behavior is consistent with the frequency shift due to the black hole growing in size. However, the growth alone does not fully account for the observed shift, though this is expected as non-trivial contribution due to non-linearities also play a role.

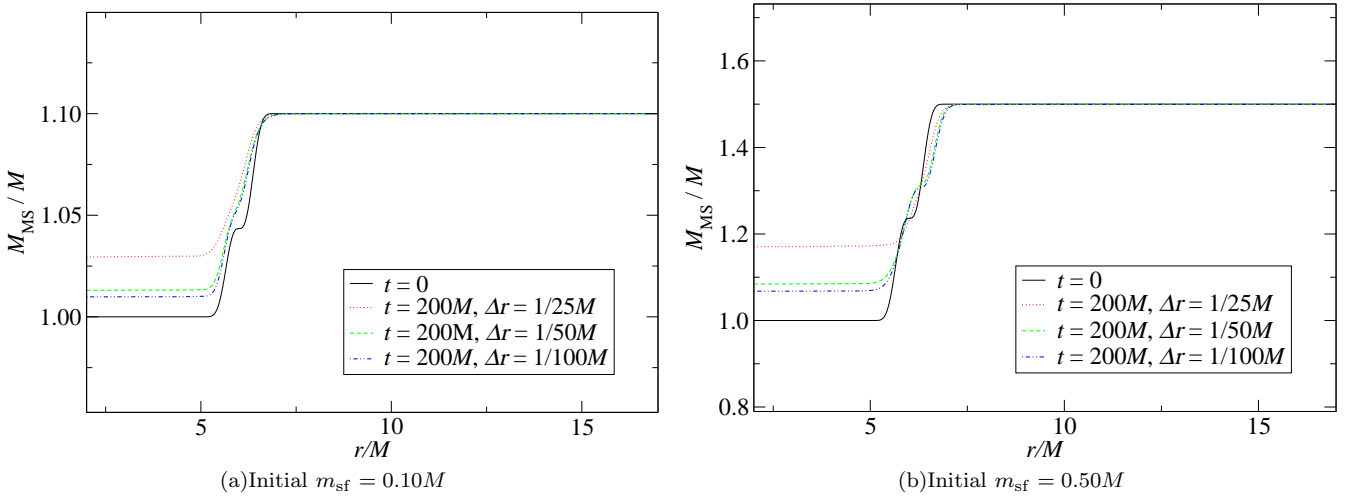


FIG. 13: Mass function at $t = 0$; and at $t = 200M$ for three resolutions. The discontinuous lines show the mass function at $t=200M$ for three resolutions. In each of these cases, about 10% of the initial mass of the scalar field falls into the black hole, while nothing escapes to infinity.

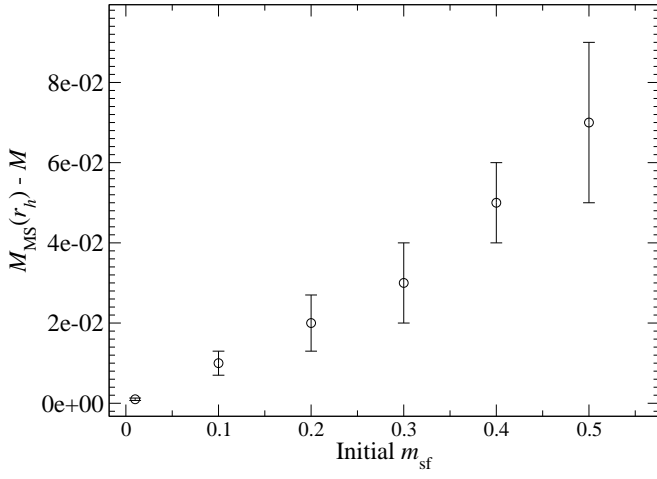


FIG. 14: Mass that falls into the black hole for different initial masses of the scalar field. Calculated as the Misner-Sharp mass at the horizon at $t = 200$ minus the initial mass of the black hole. See table I.

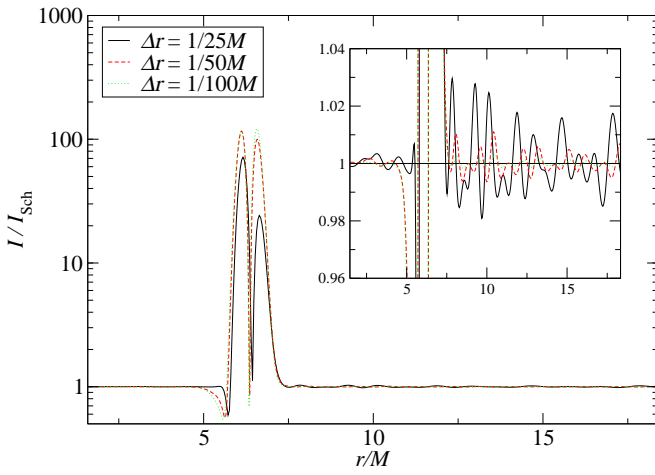


FIG. 15: Kretschmann invariant quotient for three resolutions at $t_1 = 139.983M$. This quotient converges to 1 outside of the region where the scalar field is confined. A horizontal line at $I/I_{\text{Sch}} = 1$ have been drawn as a guide. Initial $m_{\text{sf}} = 0.50M$.

VI. CONCLUSIONS

We have discussed difficulties encountered when attempting to confine a scalar field distribution within some region. The existence of a symmetry in the spacetime allows for doing so in a consistent manner. For the specific spherically symmetric case, we have given prescriptions for implementing a scalar field with a potential depending on the areal radius R .

We have illustrated the viability of this approach by confining a scalar field distribution around a black hole. For our particular choice of potential and initial scalar field, the scalar field becomes totally confined after some transient time, which depends on the initial mass. During the transient, part of the scalar field accretes into the black hole, while nothing escapes to infinity. By adjusting the depth of the potential, the amount of energy that falls in can be controlled.

The approach can be exploited, an extended, to mimic situations of interest. These can range from physical studies of particular systems, to serve as a testing model for infrastructure development aimed to simulate more complex systems.

Acknowledgments

We would like to thank M. Anderson, D. Garfinkle, C. Palenzuela-Luque, J. Pullin and R. Wald for helpful discussions as well as M. Tiglio and J. Pullin for comments and suggestions on the manuscript. This work was supported in part by NSF grants PHY-0244699, PHY-0244335, PHY0326311 and PHY0554793 to Louisiana State University. The simulations described here were performed on local clusters in the Dept. of Physics & Astronomy. L.L is grateful to the Alfred P Sloan Foundation and Research Corporation for financial support.

APPENDIX A: COORDINATE-DEPENDENT POTENTIAL IN AXIAL SYMMETRY

Following [33], we write the (general) axi-symmetric line element in the form

$$ds^2 = -e^{2\nu}(dt)^2 + e^{2\psi} (d\varphi - q_1 dx^1 - q_2 dx^2 - \omega dt)^2 + e^{2\mu_1} (dx^1)^2 + e^{2\mu_2} (dx^2)^2, \quad (\text{A1})$$

where all the functions appearing here are functions of $x^0 \equiv t$, x^1 , and x^2 , but independent of $x^3 \equiv \varphi$. We assume that the scalar field ϕ is independent of φ , and hence use H^a_b as given in (16). Evaluating $\nabla_a H^a_b$ (and assuming that h and b are independent of φ) we find that the φ -component is of the form $(h - b)$ times an expression depending on the metric functions and their derivatives. We assume that the expression multiplying $(h - b)$ is not zero, because at this moment we want to consider the case of no other symmetry other than the axial symmetry. Then, setting this component to

zero, we have the condition $b = h$, which, as we have seen earlier, implies that h is a constant. This means that the potential will be independent of the coordinates.

Consider now the special case of axial symmetry without rotation. We can write the line element in the form

$$ds^2 = g_{\varphi\varphi} d\varphi^2 + g_{ij} dx^i dx^j, \quad i, j \neq 3 \quad (\text{A2})$$

Evaluating $\nabla_a H^a_b$, the φ -component this time results identically zero, and, setting the other components to zero, we have:

$$\frac{dg_{\varphi\varphi}}{dt}(h - b) + 2g_{\varphi\varphi} \frac{dh}{dt} = 0, \quad (\text{A3})$$

$$\frac{dg_{\varphi\varphi}}{dx^1}(h - b) + 2g_{\varphi\varphi} \frac{dh}{dx^1} = 0, \quad (\text{A4})$$

$$\frac{dg_{\varphi\varphi}}{dx^2}(h - b) + 2g_{\varphi\varphi} \frac{dh}{dx^2} = 0. \quad (\text{A5})$$

At this point, one can follow the same procedures as in section II A (compare these equations to (20) and (21)). For that reason, in this section we will just summarize the results.

Equations (A3)-(A5) are satisfied if, (i): h depends on the coordinates only through an arbitrary function of $g_{\varphi\varphi}$,

$$h(t, x^1, x^2) = f(g_{\varphi\varphi}(t, x^1, x^2)), \quad (\text{A6})$$

and (ii): b is given in terms of h by

$$b = h + 2g_{\varphi\varphi} \frac{\partial h}{\partial g_{\varphi\varphi}}. \quad (\text{A7})$$

Given these conditions, one can express $\nabla_a T^a_b$ with $\nabla_b \phi$ as a common factor, and, setting it to zero, obtain the equation of motion for the scalar field,

$$\nabla_a \nabla^a \phi + \frac{\partial f}{\partial \phi} h(g_{\varphi\varphi}) = 0, \quad (\text{A8})$$

where f and h are arbitrary functions of ϕ and $g_{\varphi\varphi}$, respectively. One can, in particular, choose these functions as follows,

$$f(\phi) = -\frac{1}{2}\phi^2, \quad (\text{A9})$$

$$h(g_{\varphi\varphi}) = m^2 + U(g_{\varphi\varphi}). \quad (\text{A10})$$

Then, the evolution equation becomes

$$(\nabla_a \nabla^a - m^2 - U(g_{\varphi\varphi})) \phi = 0, \quad (\text{A11})$$

where we can interpret U as a coordinate-dependent potential.

APPENDIX B: THE EQUATIONS

The equations of motion are

$$\dot{g}_{rr} = \beta g'_{rr} + 2g_{rr}\beta' - 2\tilde{\alpha}g_{rr}^{1/2}g_T K_{rr}, \quad (\text{B1})$$

$$\dot{g}_T = \beta g'_T - 2\tilde{\alpha}g_{rr}^{1/2}g_T K_T + \frac{2\beta g_T}{r}, \quad (\text{B2})$$

$$\begin{aligned} \dot{K}_{rr} = & \beta K'_{rr} - \tilde{\alpha}g_{rr}^{-1/2}g_T f'_{rrr} - \tilde{\alpha}''g_{rr}^{1/2}g_T - 6g_T^{-1}g_{rr}^{1/2}\tilde{\alpha}f_{rT}^2 + 4g_T r^{-1}g_{rr}^{1/2}\tilde{\alpha}' - 6g_T r^{-2}g_{rr}^{1/2}\tilde{\alpha} + 2K_{rr}\beta' \\ & - g_T g_{rr}^{-1/2}\tilde{\alpha}K_{rr}^2 + 2g_{rr}^{1/2}\tilde{\alpha}K_{rr}K_T - 8g_{rr}^{-1/2}\tilde{\alpha}f_{rT}f_{rrr} + 2g_T g_{rr}^{-3/2}\tilde{\alpha}f_{rrr}^2 \\ & + 2g_T r^{-1}g_{rr}^{-1/2}\tilde{\alpha}f_{rrr} - g_T g_{rr}^{-1/2}\tilde{\alpha}f_{rrr} + g_T g_{rr}^{1/2}\tilde{\alpha}4\pi(Tg_{rr} - 2S_{rr}), \end{aligned} \quad (\text{B3})$$

$$\begin{aligned} \dot{K}_T = & \beta K'_T - \tilde{\alpha}g_T g_{rr}^{-1/2}f'_{rT} + 2\beta r^{-1}K_T + g_T r^{-2}g_{rr}^{1/2}\tilde{\alpha} + \tilde{\alpha}g_T K_T K_{rr} g_{rr}^{-1/2} - g_T f_{rT}\tilde{\alpha}'g_{rr}^{-1/2} - 2\tilde{\alpha}f_{rT}^2 g_{rr}^{-1/2} \\ & + \tilde{\alpha}g_{rr}^{1/2}g_T 4\pi(Tg_T - 2S_T), \end{aligned} \quad (\text{B4})$$

$$\begin{aligned} \dot{f}_{rrr} = & \beta f'_{rrr} - \tilde{\alpha}g_{rr}^{1/2}g_T K'_{rr} - 4g_{rr}^{3/2}\tilde{\alpha}'K_T + 12g_T^{-1}g_{rr}^{3/2}\tilde{\alpha}K_T f_{rT} - 4g_{rr}^{1/2}\tilde{\alpha}K_T f_{rrr} - g_T g_{rr}^{-1/2}\tilde{\alpha}K_{rr}f_{rrr} \\ & - 10g_{rr}^{1/2}\tilde{\alpha}K_{rr}f_{rT} + 3f_{rrr}\beta' + g_{rr}\beta'' - \tilde{\alpha}'g_{rr}^{1/2}g_T K_{rr} + 2r^{-1}g_T g_{rr}^{1/2}\tilde{\alpha}K_{rr} + 8r^{-1}g_{rr}^{3/2}\tilde{\alpha}K_T + 4\tilde{\alpha}g_{rr}^{3/2}g_T 4\pi J_r, \end{aligned} \quad (\text{B6})$$

$$\dot{f}_{rT} = \beta f'_{rT} - \tilde{\alpha}g_{rr}^{1/2}g_T K'_T + \beta' f_{rT} - \tilde{\alpha}'g_{rr}^{1/2}g_T K_T + 2g^{1/2}\tilde{\alpha}K_T f_{rT} - \tilde{\alpha}g_{rr}^{-1/2}K_T f_{rrr}g_T + 2r^{-1}\beta f_{rT}, \quad (\text{B7})$$

$$\dot{\Phi} = \beta\Phi' - \tilde{\alpha}g_{rr}^{1/2}g_T \Pi' - g_{rr}^{-1/2}\tilde{\alpha}g_T \Pi f_{rrr} + 2\tilde{\alpha}g_{rr}^{1/2}\Pi f_{rT} + 2r^{-1}\tilde{\alpha}g_{rr}^{1/2}g_T \Pi - \tilde{\alpha}'g_{rr}^{1/2}g_T \Pi + \Phi\beta', \quad (\text{B8})$$

$$\begin{aligned} \dot{\Pi} = & \beta\Pi' - g_{rr}^{-1/2}\tilde{\alpha}g_T \Phi' + g_{rr}^{-1/2}\tilde{\alpha}g_T \Pi K_{rr} + 2\tilde{\alpha}g_{rr}^{1/2}\Pi K_T - 4g_{rr}^{-1/2}\tilde{\alpha}\Phi f_{rT} + 2r^{-1}g_{rr}^{-1/2}\tilde{\alpha}g_T \Phi - g_{rr}^{-1/2}g_T \Phi\tilde{\alpha}' \\ & + g_{rr}^{1/2}g_T \tilde{\alpha}V\phi, \end{aligned} \quad (\text{B9})$$

$$\dot{\phi} = \beta\phi' - g_T g_{rr}^{1/2}\tilde{\alpha}\Pi, \quad (\text{B10})$$

$$\dot{\phi} = \beta\phi' - g_T g_{rr}^{1/2}\tilde{\alpha}\Pi, \quad (\text{B11})$$

where $\tilde{\alpha} = \alpha r^2 \sin\theta = N/\sqrt{g_{rr}g_T}$; dots denote derivative with respect to t and primes denote derivatives with respect to r ; and the ‘‘source terms’’ are defined in equations (B17)-(B21).

The constraint equations are

$$\begin{aligned} C = & \frac{f'_{rT}}{g_{rr}g_T} - \frac{1}{2r^2g_T} + \frac{f_{rT}\left(\frac{2}{r} + \frac{7f_{rT}}{2g_T} - \frac{f_{rrr}}{g_{rr}}\right)}{g_{rr}g_T} + \\ & - \frac{K_T\left(\frac{K_{rr}}{g_{rr}} + \frac{K_T}{2g_T}\right)}{g_T} + 4\pi\rho, \end{aligned} \quad (\text{B12})$$

$$\begin{aligned} C_r = & \frac{K'_T}{g_T} + \frac{2K_T}{rg_T} - \frac{f_{rT}\left(\frac{K_{rr}}{g_{rr}} + \frac{K_T}{g_T}\right)}{g_T} + \\ & + 4\pi J_r, \end{aligned} \quad (\text{B13})$$

$$C_{rrr} = g'_{rr} + \frac{8g_{rr}f_{rT}}{g_T} - 2f_{rrr}, \quad (\text{B14})$$

$$C_{rT} = g'_T + \frac{2g_T}{r} - 2f_{rT}, \quad (\text{B15})$$

$$C_m = \Phi - \phi', \quad (\text{B16})$$

where the ‘‘source’’ terms are defined as

$$4\pi\rho = \frac{V\phi^2}{2} + \frac{\Phi^2}{2g_{rr}} + \frac{\Pi^2}{2}, \quad (\text{B17})$$

$$\begin{aligned} 4\pi T = & -2V\phi^2 - \frac{\Phi^2}{g_{rr}} + \Pi^2 + \\ & - \phi^2 r^2 g_T \frac{\partial V}{\partial g_\Omega}, \end{aligned} \quad (\text{B18})$$

$$4\pi J_r = \Phi\Pi, \quad (\text{B19})$$

$$\begin{aligned} 4\pi(Tg_{rr} - 2S_{rr}) = & -V\phi^2 g_{rr} - 2\Phi^2 + \\ & - \phi^2 g_{rr} r^2 g_T \frac{\partial V}{\partial g_\Omega}, \end{aligned} \quad (\text{B20})$$

$$4\pi(Tg_T - 2S_T) = -g_T V \phi^2, \quad (\text{B21})$$

where $g_\Omega = r^2 g_T$ (see section II A).

APPENDIX C: CHARACTERISTIC STRUCTURE

The characteristic modes and eigenvalues obtained at a surface $r = \text{const}$ are given by

$$\begin{aligned} u_1 &= g_{rr}, & \lambda_1 &= \beta, \\ u_2 &= g_T, & \lambda_2 &= \beta, \\ u_3 &= K_{rr} - f_{rrr}/g_{rr}, & \lambda_3 &= \beta + \tilde{\alpha}g_T, \\ u_4 &= K_T - f_{rT}/g_{rr}, & \lambda_4 &= \beta + \tilde{\alpha}g_T, \\ u_5 &= K_{rr} + f_{rrr}/g_{rr}, & \lambda_5 &= \beta - \tilde{\alpha}g_T, \\ u_6 &= K_T + f_{rT}/g_{rr}, & \lambda_6 &= \beta - \tilde{\alpha}g_T, \\ u_7 &= \Pi + \Phi/g_{rr}, & \lambda_7 &= \beta - \tilde{\alpha}g_T, \\ u_8 &= \Pi - \Phi/g_{rr}, & \lambda_8 &= \beta + \tilde{\alpha}g_T, \\ u_9 &= \phi, & \lambda_9 &= \beta. \end{aligned} \quad (\text{C1})$$

APPENDIX D: CODE TESTS

The standard code tests have been performed, showing that all the constraints and residuals converges to

zero with order two. In figure 16 we show the Hamiltonian constraint, in the case of the strongest scalar field studied, that with initial $m_{\text{sf}} = 0.5M$.

The evaluation of the constraints is a particularly important test in this work, to ensure that the implementation of a coordinate dependent potential is not breaking the covariance of the theory.

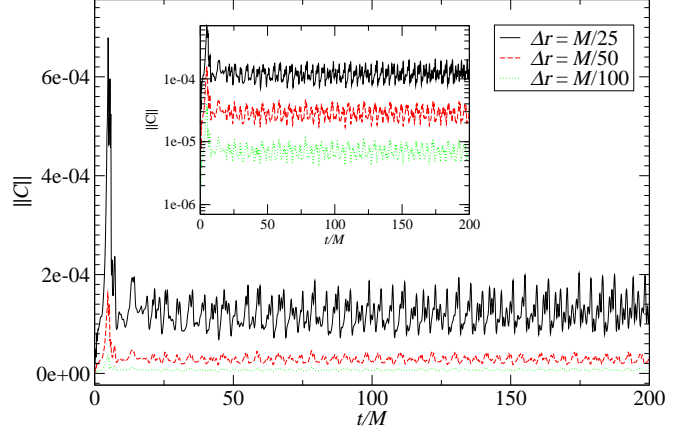


FIG. 16: L_2 norm of the Hamiltonian constraint (equation (B12)) for three different resolutions. The measured convergence results of order two as expected.

-
- [1] Misner C W, Thorne K S and Wheeler J A 1973 *Gravitation*, (New York: W H Freeman and Company)
 - [2] Scheel M A, Shapiro S L and Teukolsky S A 1994 *Phys. Rev. D* **49** 1894
 - [3] Kaup D J 1968 *Phys. Rev.* **172** 1331
 - [4] Ruffini R and Bonazzola S 1969 *Phys. Rev.* **187** 1767 .
 - [5] E. Seidel and W. M. Suen, *Phys. Rev. Lett.* **66**, 1659 (1991).
 - [6] Liddle A R (*Preprint astro-ph/9901124*).
 - [7] J. E. Lidsey, A. R. Liddle, E. W. Kolb, E. J. Copeland, T. Barreiro and M. Abney, *Rev. Mod. Phys.* **69**, 373 (1997)
 - [8] Choptuik M W 1993 *Phys. Rev. Lett.* **70** 9.
 - [9] C. Gundlach, *Adv. Theor. Math. Phys.* **2**, 1 (1998) [arXiv:gr-qc/9712084].
 - [10] Peres A 1960 *Phys. Rev.* **120** 1044
 - [11] Everson B L and Brill D R 1967 *Bull. Am. Phys. Soc.* **12** 578
 - [12] Rosen N 1940 *Phys. Rev.* **147** 150
 - [13] Kuchar K V and Torre C G 1991 *Phys. Rev. D* **44** 3116
 - [14] Choptuik M W, Hirschmann E W, Liebling S L and Pretorius F 2004 *Phys. Rev. Lett.* **93** 131101
 - [15] Olabarrieta I, Ventrella J, Choptuik M and Unruh W (Unpublished) *Critical Behavior in the Gravitational Collapse of a Scalar Field with Angular Momentum in Spherical Symmetry*
 - [16] Wald R M 1984 *General Relativity* (Chicago: The University of Chicago Press)
 - [17] Anderson A and York J W, Jr. 1999 *Phys. Rev. Lett.* **82** 4384
 - [18] Kidder L E, Scheel M A and Teukolsky S A 2000 *Phys. Rev. D* **62** 084032
 - [19] Calabrese G, Lehner L and Tiglio M 2002 *Phys. Rev. D* **65** 104031
 - [20] Press W, Flannery B, Teukolsky S and Vetterling W 1992 *Numerical Recipes in Fortran* (Cambridge University Press)
 - [21] Hindmarsh A C (Lawrence Livermore National Laboratory, <http://www.llnl.gov/casc/odepack/>)
 - [22] Kreiss H O and Scherer G 1974 in *Mathematical Aspects of Finite Elements in Partial Differential Equations*, edited by C D Boor (New York: Academic Press)
 - [23] Kreiss H O and Scherer G 1977 *Tech. Rep. Dept. of Scientific Computing*, Uppsala University
 - [24] Strand B, 1994 *Journal of Computational Physics* **110** 47
 - [25] Calabrese G, Lehner L, Neilsen D, Pullin J, Reula O, Sarbach O and Tiglio M 2003 *Class. Quant. Grav.* **20** L245
 - [26] Calabrese G, Lehner L, Reula O, Sarbach O and Tiglio M 2004 *Class. Quant. Grav.* **21** 5735
 - [27] Levy D and Tadmor E 1998 *SIAM Journal on Num. Anal.* **40** 40
 - [28] Kreiss H and Olinger J 1973 *Methods for the approximate solution of time independent problems* (Geneva: GARP Publication Series)
 - [29] Gustafsson B, Kreiss H and Olinger J 1995 *Time dependent problems and difference methods* (John Wiley and

- Sons)
- [30] Lehner L, Neilsen D, Reula O and Tiglio M 2004 *Class. Quant. Grav.* **21** 5819
 - [31] Olsson P 1995 *Math. Comp.* **64** 1035; **64** S23; **64** 1473
 - [32] Thomas J W 1995 *Numerical Partial Differential Equations: Finite Difference Methods*, Texts in Applied Mathematics 22 (New York: Springer-Verlag)
 - [33] Chandrasekhar S 1992 *The Mathematical Theory of Black Holes* (New York: Oxford University Press)
 - [34] This equation can be thought just as the definition of the tensor A^a_b
 - [35] Suggested by the fact that in Schwarzschild coordinates, (\tilde{t}, \tilde{r}) , the ansatz $\phi = u(\tilde{r}) \cos(\omega \tilde{t})$ yields separation of variables. The coordinates transformation being: $\tilde{t} = t - 2M \ln\left(\frac{r-2M}{M}\right)$, $\tilde{r} = r$.
 - [36] The position of the apparent horizon is given by the outermost trapped surface.